

Kinetics and mechanisms of precipitation in an Al–0.2 wt.% Sc alloy

Jostein Røyset*, Nils Ryum

Department of Materials Technology, Norwegian University of Science and Technology, N-7491 Trondheim, Norway

Received 1 October 2004; received in revised form 2 February 2005; accepted 9 February 2005

Abstract

Specimens of an Al–0.2 wt.% Sc alloy were solution heat treated and isothermally annealed in the temperature range of 190–530 °C, and the precipitation reaction was followed with electrical conductivity measurements. Some specimens were also examined by using light microscopy and transmission electron microscopy. The conductivity measurements were used to characterise the kinetics of the transformation, and a TTT (time–temperature–transformation) diagram was constructed. Two transformation time minima are observed, one at about 310 °C, which is associated with continuous precipitation and the other at about 410 °C which is associated with discontinuous precipitation. Conductivity measurements from the coarsening stage were used for estimating the solvus line of the phase diagram and the interface energy between Al and Al₃Sc. Good solvus estimates were achieved in the temperature range of 370–530 °C. The estimates of interface energy spread from approx. 20 to 300 mJ/m².

© 2005 Elsevier B.V. All rights reserved.

Keywords: Al–Sc; Electrical conductivity; Transformation kinetics; Precipitation mechanisms; Solvus line; Interfacial energy

1. Introduction

Scandium (Sc) is considered as a promising alloying element in aluminium (Al) alloys, and it has been shown that a small Sc-addition can improve a range of material properties in a range of Al-alloy systems [1–7]. Most of the beneficial effects from the Sc-addition are linked to the formation of the Al₃Sc phase in the alloy. In a typical processing route of a wrought aluminium alloy particles of the Al₃Sc phase can form under three different conditions, each of which influences the microstructure and properties of the alloy in a specific way:

1. During solidification after casting or welding, Al₃Sc particles can form in the melt and act as grain refiners. This requires that the alloy is hypereutectic with respect to Sc. For a binary Al–Sc alloy this means that the Sc content should be in excess of approx. 0.6 wt.% [8], while in for

instance an Al–Zn–Mg–Zr alloy an addition of 0.2 wt.% Sc can be sufficient [9,10].

2. High temperature processing of the alloy in the range of 400–600 °C, for instance homogenisation, hot-rolling or extrusion, can give a dense distribution of Al₃Sc particles. Typical particle diameters from such processes would be in the range of 20–100 nm. These particles will not have a significant direct strengthening effect on the alloy, but they will have a stabilising effect on the grain structure/subgrain structure of the alloy. Good recrystallization resistance [11–13] and enhanced superplasticity [9,14,15] of Sc-containing alloys are properties that are attributed to the distribution of Al₃Sc particles formed under conditions as mentioned above.
3. Heat treatment in the range of 250–350 °C can lead to significant precipitation hardening of an alloy supersaturated in Sc [1,2,11]. The size of strengthening Al₃Sc precipitates is typically in the range of 2–6 nm [16], and the precipitates are reported to be completely coherent with the aluminium matrix [17].

* Corresponding author. Present address: Hydro Aluminium R&D Sunndal, Romsdalsvegen 1, N-6600 Sunndalsøra, Norway. Tel.: +47 71 69 36 04; fax: +47 71 69 36 02.

E-mail address: jostein.royset@hydro.com (J. Røyset).

This investigation deals with the formation of Al₃Sc when the alloy is in the solid state, i.e. related to points (2) and (3)

above. It has been reported that Al_3Sc particles can form from a supersaturated solid solution in two different ways:

1. Precipitation as described by classical theory of nucleation and growth [18,19]. To the author's knowledge, no observations of GP-zones or transient phases prior to the formation of Al_3Sc have been reported. It is thus assumed that the Al_3Sc phase nucleates directly from the supersaturated solid solution. For convenience, this precipitation mechanism is referred to as "continuous precipitation" in this paper.
2. Discontinuous precipitation [18,20–22]. By this mechanism, the supersaturated solid solution decomposes to a less supersaturated solid solution and Al_3Sc particles behind a moving grain boundary. Precipitates formed by this mechanism are easily identified due to their arrangements in fan-shaped patterns.

In general, discontinuous precipitation leads to a coarser and less uniform particle distribution than does continuous precipitation. Factors that are known to influence the tendency to discontinuous precipitation are Sc-level, precipitation temperature and presence of other alloying elements.

Scandium is quite expensive. In order to minimise the Sc-addition that is needed to give the desired effects in an alloy, it is necessary to be able to predict the modus and kinetics of the formation of Al_3Sc particles from a supersaturated solid solution. Several investigations of the precipitation kinetics and precipitation mechanisms of Al_3Sc have been published in the technical literature over the past 10–20 years [16–20,22–33]. The published material does, however, give only a limited overview of the regimes in which either of the two precipitation mechanisms occur, and the differences in precipitation kinetics between the two mechanisms are not accounted for. The aim of the present investigation is to provide more information about these issues by studying the isothermal precipitation behaviour of a binary Al–Sc alloy over a wide temperature range.

2. Experimental procedure

The alloy studied in this investigation was a binary Al–0.2 wt.% Sc alloy. First, an Al–0.6 wt.% Sc master alloy was prepared from superpure (99.999%) Al and 98% pure Sc. Sc-chips were added to the Al-melt at 800 °C under an inert atmosphere. The melt was kept at that temperature for 90 min, and stirred every 30 min. A graphite mould was used for casting the master alloy. After checking that the alloying was successful, a portion of the master alloy was diluted by superpure Al to an Al–0.2 wt.% Sc alloy. This alloy was cast into rod-shaped graphite moulds with a diameter of 12 mm.

The Sc content of the alloy was checked by EDS analysis in a Philips XL 30S FEG-SEM equipped with an EDAX detector. This particular analysis was estimated to be accurate within ± 0.02 wt.%. The trace element content was checked

by an optical emission spectrograph with a detection limit of approx. 10 ppm.

Slices of approx. 1.5 mm thickness were cut from the rods. These specimens were solution heat treated in a molten salt furnace at 600 °C for 1 h, and quenched directly from this temperature to the precipitation temperature either in an oil bath or in another molten salt furnace. A wide range of precipitation temperatures was applied: 190–530 °C, with 20 K intervals. At each temperature, specimens were kept for about 25–45 different time intervals and subsequently water-quenched. The resulting electrical conductivity was measured by a Sigmascope eddy current apparatus at room temperature. Two measurements were made on each specimen: one on each side of the disc. In order to save material, the specimens were re-solutionized and precipitation heat treated several times.

For selected temperatures and precipitation times, specimens were prepared for light microscope studies and TEM studies by standard techniques. These specimens were of "virgin" material, i.e. solution heat treated and precipitation heat treated only once. The TEM studies were done in a JEOL JEM 2010 with an acceleration voltage of 160 kV.

3. Results and discussion

3.1. Measurements of electrical conductivity

The EDS analysis of the Al–Sc alloy gave a composition of 0.23 wt.% Sc, and the total impurity content of the alloy was less than 200 ppm (see Table 1). Looking at the Al-side of the binary Al–Sc phase diagram as determined by [34], one finds that the solvus concentration at the applied solutionizing temperature of 600 °C is 0.22 wt.%, which is slightly less than the measured Sc content in the alloy (0.23 wt.%). Ideally, a higher solutionizing temperature should have been used but the salt bath furnace temperature could not be increased above 600 °C. One did, however, not observe retaining particles from the solution heat treatment in TEM. Considering the uncertainty of the chemical analysis, the temperature measurements and of the assessment of the solvus line, one chose to assume that the solution heat treatment brought all the Sc into solid solution. The electrical conductivity of specimens after solution heat treatment was consistently 32.2 ± 0.1 MS/m, and this number was used as an indication that all Sc was in supersaturated solid solution.

Table 1
Scandium content and impurity levels in the alloy

Element	wt.%
Sc	0.23
Cu	0.002
P	0.003
Pb	0.001
Si	0.010
Ti	0.002
Other	<0.001

Table 2
Electrical resistivity ρ due to Sc atoms in solid solution

Reference	ρ [n Ω m/at. %]	Note
Ocko et al. (1976) [36]	35 \pm 5	Measured at 4.2 and 273 K
Fujikawa et al. (1979) [34]	34 \pm 1	Measured at -196°C (77 K)
Berger (1980) [37]	23 \pm 2	Measured at 1.6 K, very dilute alloy
Papastaikoudis and Papadimitropoulos (1981) [38]	53.2–82	Measured at 4.2 K, very dilute alloys
Hatch [39]	33.2	
Torma et al. (1985) [40]	44 \pm 1	Measured at -196°C (77 K)
Sano et al. (1987) [17]	38	Measured at -196°C (77 K)
This work	29.7	Measured at room temperature (about 295 K)

Shortly after the specimens are quenched from the solutionizing temperature to the precipitation temperature, the average Sc-concentration C_{Sc} in the Al-matrix will decrease as the Al_3Sc particles nucleate and grow. The electrical conductivity of the alloy will increase accordingly. Electrical resistivity is the inverse of electrical conductivity, i.e.

$$\rho = \frac{1}{\sigma} \quad (1)$$

where ρ is electrical resistivity and σ the electrical conductivity. It is in general found that the electrical resistivity ρ of binary Al-alloys is increasing proportionally with the solute content C [35], and it has been demonstrated that this is also the case for dilute Al–Sc alloys [34]. The isothermally transformed fraction $X(t)$ after a time t can thus be expressed as¹

$$\begin{aligned} X(t) &= \frac{C_{\text{Sc}}^0 - C_{\text{Sc}}(t)}{C_{\text{Sc}}^0 - C_{\text{Sc}}^T} = \frac{\rho_{\text{Sc}}^0 - \rho_{\text{Sc}}(t)}{\rho_{\text{Sc}}^0 - \rho_{\text{Sc}}^T} \\ &= \frac{(1/\sigma_{\text{Sc}}^0) - (1/\sigma_{\text{Sc}}(t))}{(1/\sigma_{\text{Sc}}^0) - (1/\sigma_{\text{Sc}}^T)} \end{aligned} \quad (2)$$

where C_{Sc}^0 is the Sc content of the alloy, $C_{\text{Sc}}(t)$ the Sc content in the aluminium matrix at the time t , and C_{Sc}^T the equilibrium concentration of Sc in the Al-matrix at the precipitation temperature. The indexing of ρ and σ follows the same pattern.

At the end of the transformation, the average Sc content in solid solution should be close to the solvus concentration in the binary phase diagram. The conductivity of superpure Al at room temperature was measured to be 37.0 MS/mm, which corresponds to an electrical resistivity of 27.0 n Ω m. Solutionized specimens had a conductivity of 32.2 MS/m, corresponding to 31.1 n Ω m. Thus, one assumes that the effect of Sc in solid solution on the electrical resistivity amounts to 17.8 n Ω m/wt. % Sc (29.7 n Ω m/at. % Sc). This value is in the same range as what has been found in other investigations [17,34,36–40] (Table 2).

¹ Some results from this investigation were presented at the ICAA6 Conference in Toyohashi, Japan, in 1998 [22]. In that paper, it was assumed that the electrical conductivity increases proportionally with the decrease in solute content. This is a clearly erroneous assumption. Some minor deviations in results between the ICAA6-paper and the present paper are due to that particular error.

3.2. Kinetics of the precipitation reaction

Some examples of transformation/time plots calculated from the conductivity measurements are shown in Fig. 1. For the temperatures up to 350 $^\circ\text{C}$ the curves have a sigmoidal shape. At 370 $^\circ\text{C}$ there is a marked shift to a slower transformation rate in the late stage, and for higher temperatures this shift to a slower transformation rate moves to earlier stages of transformation. At 490 $^\circ\text{C}$ the entire transformation occurs at the slow rate.

The Johnson–Mehl–Avrami–Komalgorov (JMAK) relationship is often used to describe the kinetics of isothermal phase transformations, whereby the fraction transformed, $X(t)$, is expressed as

$$X(t) = 1 - e^{-k(Dt)^n} \quad (3)$$

where k is a constant, D the interdiffusion constant of Sc in Al, and n is dependent on the nucleation mechanism [41]. To check whether the JMAK relationship applies for the precipitation reaction one can plot the measured data as ‘ $\log \ln(1/(1-X))$ ’ versus ‘ $\log t$ ’. In this paper, such plots are referred to as “JMAK-plots”. If the JMAK relationship is valid, the data should make up a straight line with a slope equal to n . In the idealised case that all particles nucleate simultaneously at random sites the value of n will be 3/2. If the nucleation rate is constant during the transformation, however, the value of n will be 5/2 [41].

Some examples of JMAK-plots are shown in Fig. 2. In the start and end of the transformation the data do not fit very well with Eq. (3). Thus, the present JMAK-plots are made only for transformation degrees X between approx. 0.05 and 0.95. In this interval, however, the data sets are describing straight lines. In the temperature range of 370–470 $^\circ\text{C}$ the data points seem to make up two straight lines rather than just one. It is reasonable to assume that these observed shifts in transformation rates are related to shifts in transformation mechanisms and given the rather abrupt changes in slope between the two lines it seems that the two mechanisms are consecutive, i.e. that the two transformation mechanisms do not overlap in time.

Fig. 3 shows a plot of the observed n values as a function of transformation temperature. In the temperature range of 250–350 $^\circ\text{C}$, the measured n values are in the range of 1.5–1.8. According to Christian [41] this is close to what one

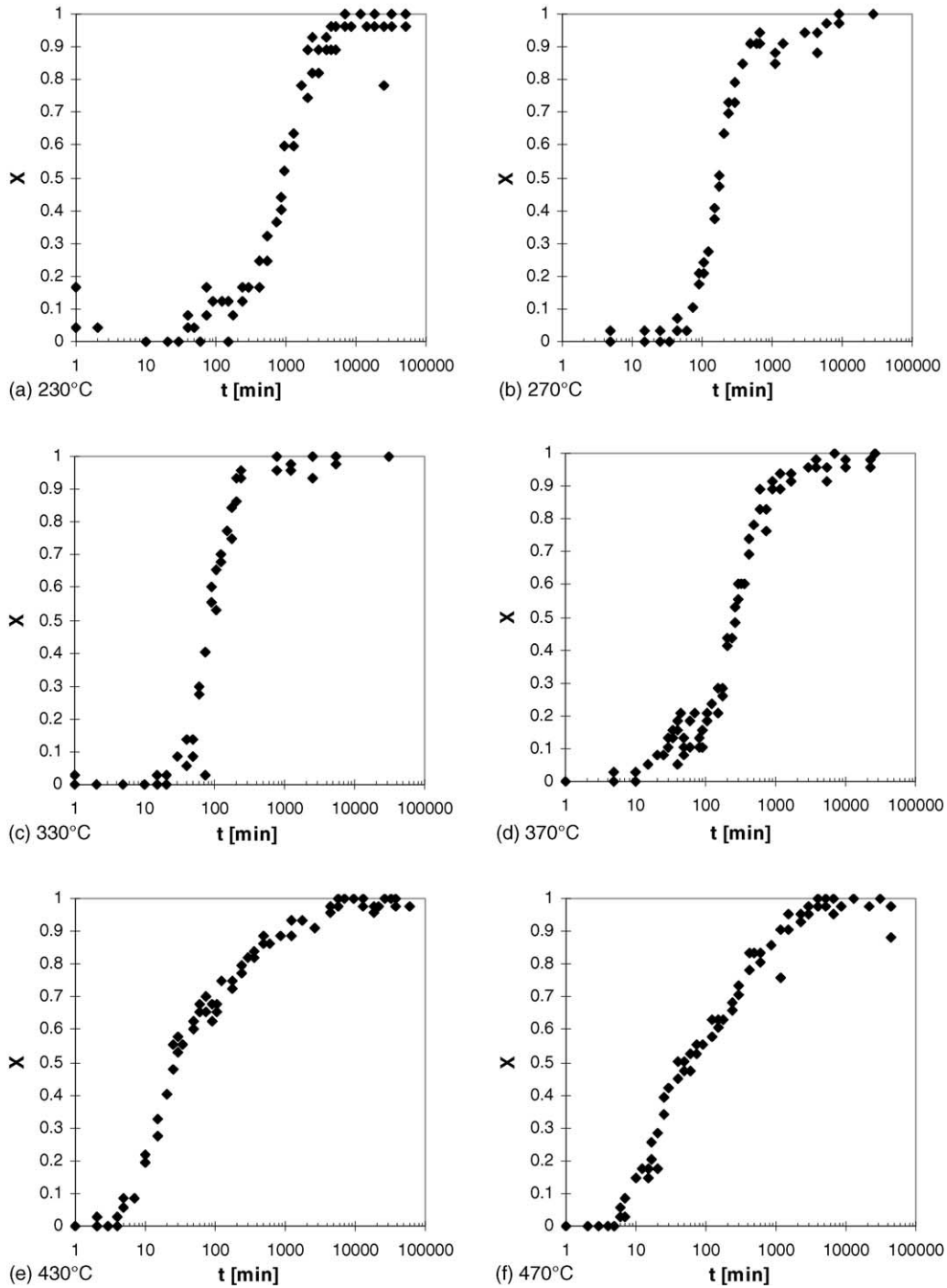


Fig. 1. Fraction transformed, derived from electrical conductivity measurements, as a function of isothermal transformation time.

would expect in the case where all the precipitates nucleate simultaneously at random sites, but one should keep in mind that the observation of a n value in this range is not per se a proof of such a nucleation condition. In the temperature range of 370–470 °C the n values of both transformation stages are plotted. In the first stage, the measured n value is in the range of 1.2–1.5. For the second transformation stage one cannot read the n value directly from the plots of Fig. 2. The fraction transformed $X(t) = 0$ has to be assigned to the value of electri-

cal conductivity where the onset of the second transformation stage is observed to take place, and new JMAK plots must be made. The n values of the second stage are extracted through such a procedure. These values lie within the range of 0.5–1, and there seems to be an increase in n value with increasing transformation temperature.

Values of n reported in other investigations [19,27,32] are given in Table 3. In all these investigations, however, the specimens were brought to the transformation temperature from

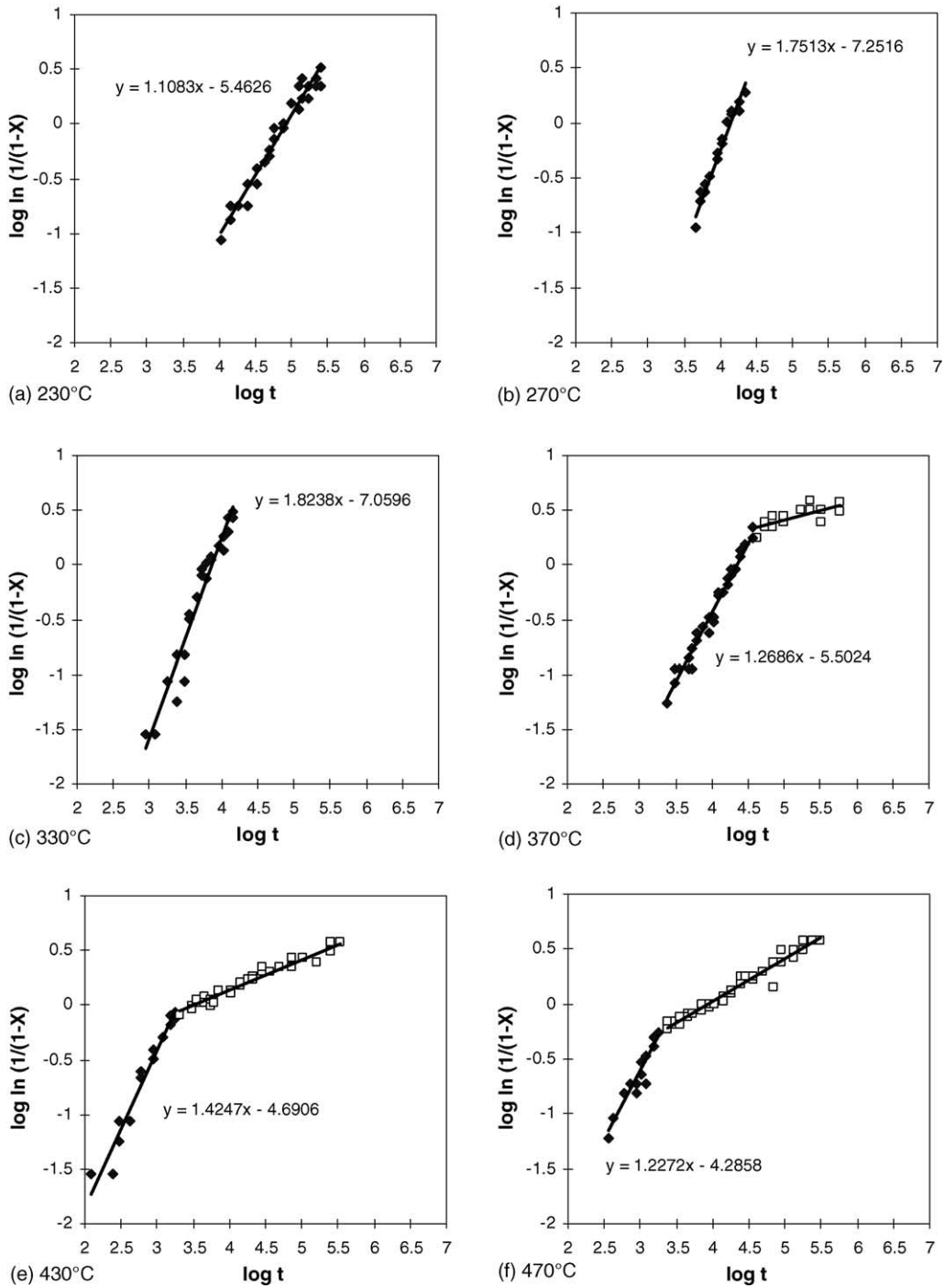


Fig. 2. Johnson–Mehl–Avrami–Komolgorov (JMAK) plots of the transformation curves of Fig. 1.

Table 3
Values of n in the JMAK equation reported in previous works

Reference	n	C_{Sc}^0 [wt.% Sc]	T_{trans} [°C]	Note
Berezina et al. (1990) [27]	1.3	0.30	300	Solution heat treated (SHT) 500 °C
	1.6/0.26	0.30	300	SHT 600 °C, low n at late stage
	2.0/0.26	0.30	300	SHT 640 °C, low n at late stage
Jo and Fujikawa (1993) [19]	1.30–1.49	0.15	260–370	
	1.45–1.96	0.25	260–370	
Fujikawa and Sakauchi (1998) [32]	1.88–2.16	0.20	240–350	

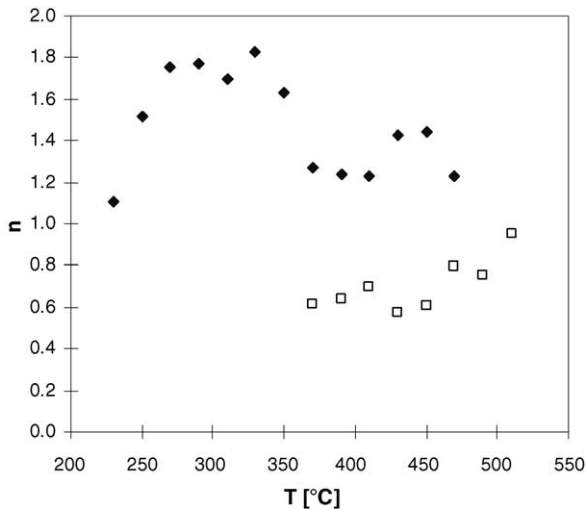


Fig. 3. The n values of the JMAK plots as a function of temperature: (◆) rapid stage, (□) slow stage.

room temperature, not from a solutionizing temperature as was the case in the present investigation. Thus a direct comparison between the present result and the results in Table 3 may not be relevant.

The essential data from the transformation curves are summarised in a TTT (time–temperature transformation) diagram of Fig. 4. Three iso-transformation lines are plotted; for 5, 50 and 95% of the overall transformation as defined by Eq. (2). As one can see there are two distinct local minima in transformation time, one at approx. 310 °C and the other at approx. 410 °C. Normally, different transformation time minima at different temperatures indicate that the operating transformation mechanisms are not the same at each minimum.

A comparison with other reported TTT-diagrams in the technical literature [19,21,31] does not show the same, clear division into two transformation time minima, although there is some deviation from an ideal c-shape. It is recognised in [19] that there is a difference in transformation kinet-

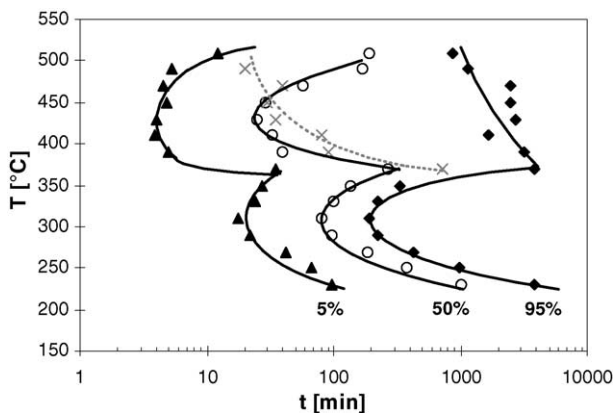


Fig. 4. Time–temperature–transformation (TTT) diagram based on the JMAK plots: (▲) 5% transformation, (○) 50% transformation, (◆) 95% transformation, (×) point of transition from rapid stage to slow stage of transformation (indicated by stippled line).

ics between the low-temperature and the high-temperature regime. Fig. 7 of reference [28] contains essentially the same type of information as a TTT-diagram. Here, two transformation time minima are very clearly observed. Both [19] and [28] link the differences in kinetics between the low- and the high-temperature regime to observations of coherent Al_3Sc particles at low temperatures and incoherent Al_3Sc particles at high temperatures. Once again it must be stressed that all these investigations are based on specimens that were water-quenched prior to isothermal annealing, and that a direct comparison with the present result may not be valid.

3.3. Microstructural evolution during isothermal transformation

Due to the low Sc content and the lack of other impurities in the alloy, the grain size of the as-cast material was quite large. The grains were columnar, and the largest ones would run almost from the surface and to the centre of the cast rod. Fig. 5(a) shows the centre of a disk of the as-cast material. The solution heat treatment at 600 °C leads to some coarsening of the grain structure. As can be seen from Fig. 5(b), the grain boundaries are also smoother.

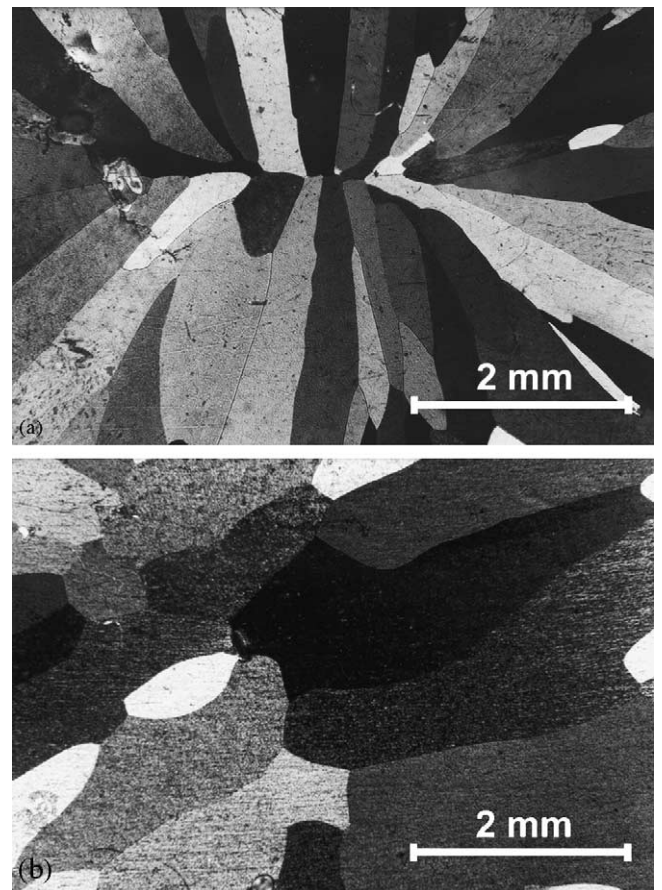


Fig. 5. Microstructure of the specimens: (a) in the as-cast state and (b) in the as-solution heat treated state.

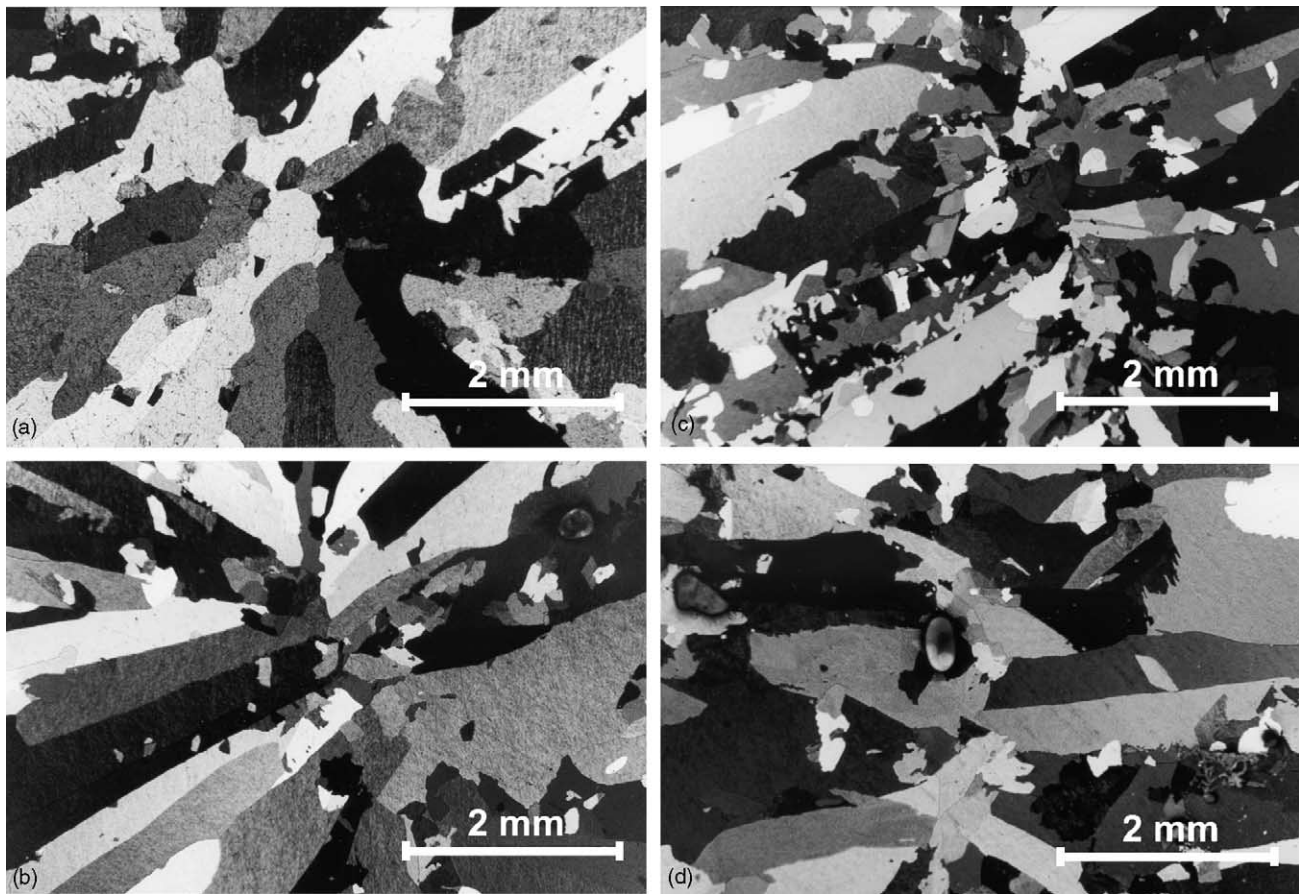


Fig. 6. Microstructural evolution during isothermal ageing at 450 °C: (a) 10 min, (b) 20 min, (c) 1 h, (d) 4 h.

Specimens annealed at 450 or 350 °C for various times were studied in light microscope and TEM.

There is a distinct evolution of the grain structure of the specimens during annealing at 450 °C. In specimens annealed for 5 min one finds that a few of the grain boundaries have a ragged shape. This feature is even more evident after 10 min, and can be seen in Fig. 6(a). Looking closely, the grain structure seems to evolve in three distinct manners:

1. neighbouring grains start protruding into each other;
2. new grains are formed on old grain boundaries;
3. new grains are formed within old grains.

The mutually protruding grain boundaries often have a wavy shape, while the newly formed grains often have one or more linear boundaries with the old grains. The character of some of these boundaries, as for instance the row of triangles on the right side of Fig. 6(a), clearly indicates that there exist preferential orientation relationships between the old grains and the new ones.

There are some specimen-to-specimen variations as for the evolution of area fraction new grains with annealing time. For instance, the specimen annealed for 30 min seem to have much fewer new grains than the specimen annealed for 20 min. The overall trend is, however, that the area fraction

of new grains increases with annealing times for times up to 60 min. For longer annealing times it is not possible to detect an increase in the area fraction of new grains.

Looking at the TTT-diagram Fig. 4, the apparent halt in formation of new grains is relatively close to the observed shift in transformation kinetics at 450 °C.

An investigation in TEM reveals that the initial part of the transformation occurs by discontinuous precipitation. Fig. 7(a) shows from a specimen annealed at 450 °C for 10 min. A grain boundary runs diagonally across the picture, and there is a fan-shaped array of precipitates on one side of the grain boundary. This is a typical arrangement for precipitates that are formed by discontinuous precipitation. No other precipitates were observed outside the discontinuously transformed areas.

The same fan-shaped arrays of precipitates were found in the specimen aged at 450 °C for 60 min, as shown in Fig. 7(b). In this specimen, however, some Al₃Sc precipitates were observed outside the discontinuously transformed areas. Some of them are weakly visible on the left side of the grain boundary of Fig. 7(b).

The observed discontinuous precipitation is obviously the underlying cause of the evolution of grain structure during annealing at 450 °C: this precipitation mechanism can only

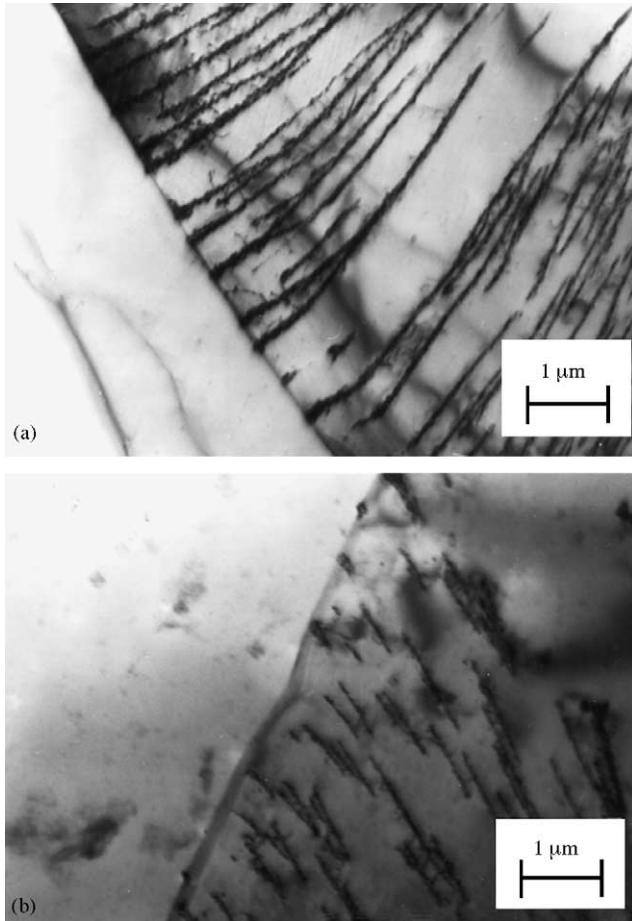


Fig. 7. Transmission electron microscope (TEM) images of discontinuous precipitation in specimens annealed at 450 °C: (a) 10 min, (b) 1 h.

be operating if grain boundaries are moving. It seems that the Al_3Sc particles precipitate both discontinuously and continuously, and that the discontinuous precipitation start first. It is plausible that the continuously precipitated particles, as they start to appear in the non-transformed volume, interrupt the discontinuous precipitation. There will be two negative effects on the discontinuous precipitation:

1. The growth of continuously precipitated Al_3Sc particles depletes the nearby matrix for Sc, and thus reduces the driving force for discontinuous precipitation.
2. Continuously precipitated Al_3Sc particles impose a Zener-drag on the advancing grain boundaries, and thus impede the discontinuous precipitation.

It is tempting to relate the observed shift in n value in the JMAK-plots of Fig. 2 to the apparent halt in discontinuous precipitation. Considering the JMAK-plot for 450 °C, one can attribute the first, steep line to the stage where discontinuous precipitation takes place, and the second, less steep line to the transformation that occurs after the discontinuous precipitation comes to a halt.

Incidentally, it is an interesting point that the observed discontinuous precipitation can also be viewed as an analog to a

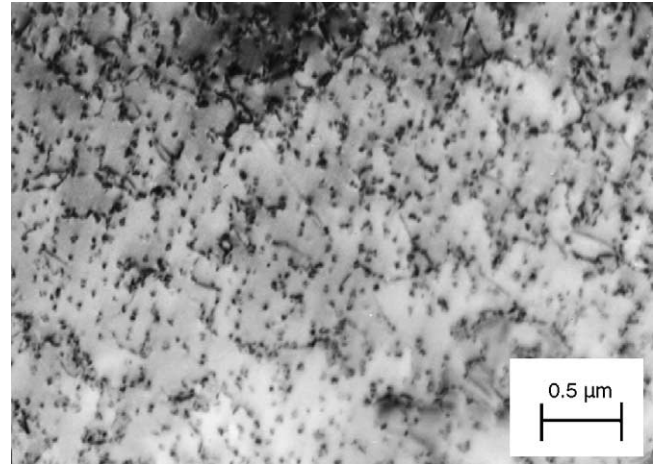


Fig. 8. TEM image of the Al_3Sc precipitates after 4 h annealing at 350 °C.

recrystallisation reaction. By measuring the evolution of the transformed volume over time as observed in the light microscope, it should also be possible to make a JMAK analysis on these data. However, the present work does not provide enough data for such an analysis.

A TEM study of the specimen annealed at 350 °C for 240 min. revealed a uniform distribution of fine-scale Al_3Sc precipitates throughout the specimen volume, as shown in Fig. 8. No fan-shaped arrays of precipitates were found. Looking at the same sample in a light microscope one did not find evidence of discontinuous precipitation. Thus one concludes that the Al_3Sc particles form by continuous precipitation at this temperature.

Looking at the TTT-diagram of Fig. 4, it is reasonable to assume that the two transformation time minima and their adjacent temperature regimes correspond to the two observed precipitation mechanisms: continuous precipitation at the lower temperatures and discontinuous precipitation at the higher temperatures. Fig. 9 shows a tentative summary of which transformation mechanisms that are believed to be dominating in the various temperature/time regimes.

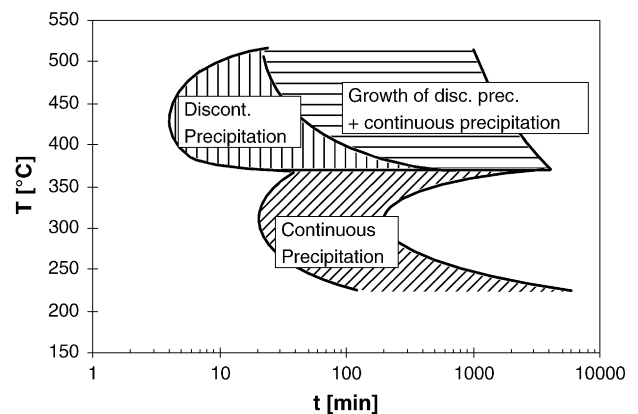


Fig. 9. Tentative map of isothermal transformation mechanisms.

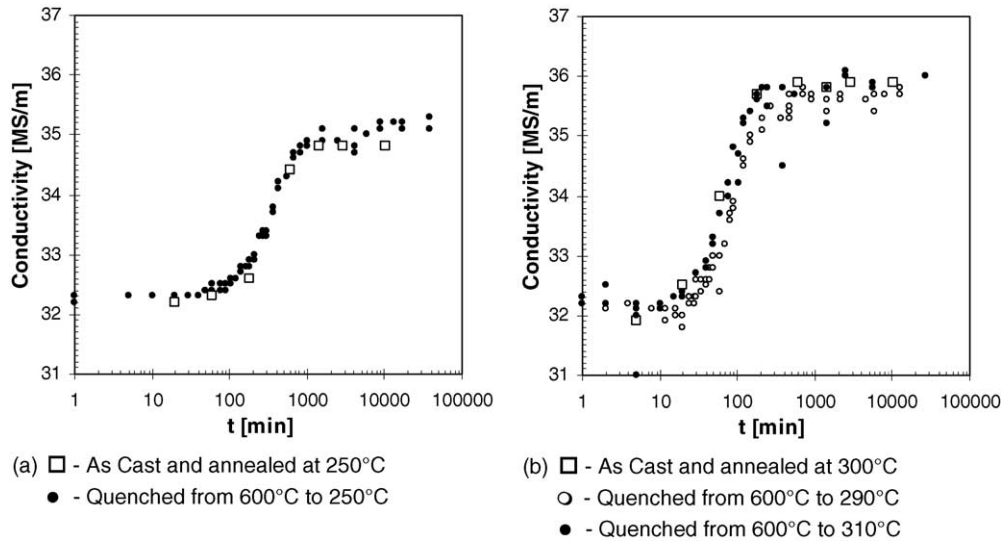


Fig. 10. Comparison of electrical conductivity of as-cast and aged specimens versus specimens that are solution heat treated and directly quenched to the transformation temperature.

3.4. Effect of room temperature storage on precipitation kinetics

The alloy used in this investigation was also used in another work, parts of which is published in [11]. In that work, as-cast material was age hardened at 250 and 300 °C. The material was stored at room temperature between casting and age hardening: 1 day before age hardening at 300 °C and 17 days before age hardening at 250 °C. The measured electrical conductivities are plotted along with the measurements of the present investigation in Fig. 10. (No measurements at 300 °C were made in this investigation, therefore the data sets of 290 and 310 °C are used for comparison.)

As one can see, there is a practically perfect match between the data of the two investigations. This means that room temperature storage versus direct quench to precipitation temperature does not make any measurable influence on the precipitation kinetics of this alloy.

In another investigation, the effect of direct quench to age hardening temperature versus water quench and subsequent age hardening was investigated [18]. Here, the onset of precipitation came much earlier in the specimens that were water-quenched prior to age hardening. This shift in incubation time was assumed to be due to quenched in vacancies, which enhance the diffusivity of Sc in the alloy. The specimens used in [11], however, were not water-quenched. The as-cast material was cooled in the graphite mould it was cast in, which took several minutes. This should lead to only negligible vacancy supersaturation in the specimens as they reached room temperature.

3.5. Extrapolation of coarsening data for determination of the solvus line

Assuming that the isothermal coarsening of Al₃Sc precipitates is governed by volume diffusion, the process should be

described by the Lifshitz–Slyozow–Wagner equation:

$$r^3 = r_0^3 + k'(t - t_0) \tag{4}$$

where r is the average particle radius at the time t , and r_0 the average particle radius at the onset of coarsening at the time t_0 . Following the reasoning of for instance [42], it is possible to deduce the following equation for how the solute concentration C_{Sc} varies with the time:

$$C_{Sc}(t) = C_{Sc}^T + kt^{-1/3} \tag{5}$$

It has been demonstrated that the method of applying isothermal coarsening data to Eq. (5) and extrapolating to $t = \infty$ yields a good estimate for the solvus concentration in several binary alloy systems, including the Al–Sc system [43]. This method was applied to the conductivity measurements of this investigation. For each transformation temperature the apparent measured concentration $C_{Sc}(t)$, which can be derived from Eq. (2), was plotted against $t^{-1/3}$ and linear regression was applied to the coarsening stage of the transformation. The intercept of the regression line with the C -axis should thus be an estimate for the solvus concentration at that temperature.

Table 4 gives the resulting solvus estimates, which are also plotted in Fig. 11. For temperatures of 370 °C and above the present solvus estimates increase with increasing temperature, and the data points are within the spread of previously reported values [19,26,33,34,44–49]. It thus seems that the current estimates are good in this temperature regime.

Assuming a regular solution, the solid solubility of Sc in Al can be described by the equation:

$$C'_{Sc} = \exp\left(\frac{\Delta S}{R}\right) \exp\left(-\frac{\Delta H}{RT}\right) \tag{6}$$

where ΔS and ΔH are the changes in entropy and enthalpy, respectively, when 1 mol of Sc is mixed with Al to make a dilute solid solution and C'_{Sc} the solvus concentration ex-

Table 4
Solvus concentrations obtained by extrapolating coarsening data to infinite time

T [°C]	C_{Sc}^T [wt.%]	Note
530	0.0975	
510	0.0724	
490	0.0596	
470	0.04	
450	0.0331	
430	0.0281	
410	0.0181	
390	0.0138	
370	0.0097	
350	0.0242	Not a correct estimate of solvus
330	0.0321	Not a correct estimate of solvus
310	0.0406	Not a correct estimate of solvus
290	0.0516	Not a correct estimate of solvus
270	0.0601	Not a correct estimate of solvus
250	0.0721	Not a correct estimate of solvus
230	0.0877	Not a correct estimate of solvus
190	0.126	Not a correct estimate of solvus

pressed as atomic fraction of Sc, R the gas constant and T the temperature in K [50]. Thus, plotting $\ln(C_{Sc}^T)$ against $1/T$ should yield a straight line with the slope $-\Delta H/R$ and which intercepts the $\ln(C_{Sc}^T)$ -axis at a value corresponding to $\Delta S/R$. In Fig. 12, this is done for the present solvus estimates at 370 °C and above. As one can see the data points describe a fairly straight line, indicating that the solid solution of Sc in Al is of a regular nature. A linear regression line is applied to the data points. In order to get more precise estimates of ΔS and ΔH , and thus the solvus line, one chose to fix the regression line at the point of maximum solid solubility. The values 0.23 at.% (0.38 wt.%) and 660 °C of the assessed phase diagram in [46] are used. This gives the values of 19 J/mol K and 65 kJ/mol for ΔS and ΔH , respectively. Table 5 gives an overview of other reported data on ΔS and ΔH in the literature [19,33,34,39,40,51,52]. There is reasonable agreement

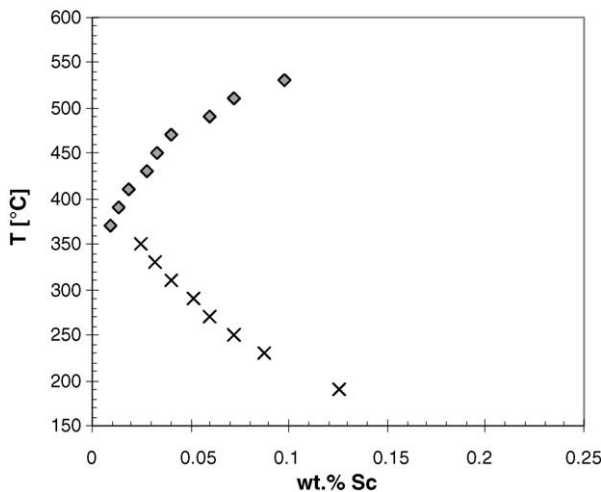


Fig. 11. Estimates of solvus concentrations from extrapolation of coarsening data: (♦) good estimates, (×) estimates that deviate from the expected solvus shape.

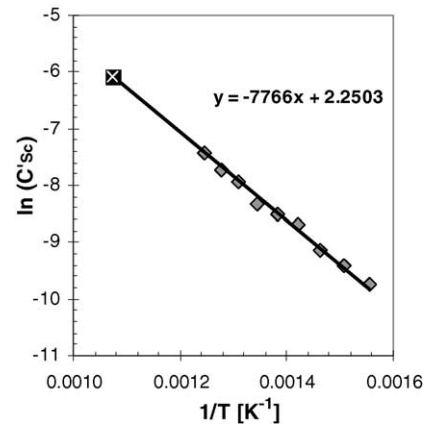


Fig. 12. Fit of the solvus estimates to Eq. (6).

between the present estimate and the literature data.² The regression line of Fig. 12 is used as an estimate of the solvus line in Fig. 13. Also shown in Fig. 13 are the data points of the solvus line as determined in the present and in other experimental investigations.

3.6. Estimates of the particle/matrix interface energy from coarsening data

The slope k of the curve given by Eq. (5) can be used for estimating the interface energy γ between the Al_3Sc particles and the Al matrix. This method has also been applied in [19], where the constant k is given as

$$k = \left(\frac{9\gamma^2(C_T^*)^2 V_m}{D(RT)^2} \right)^{1/3} \quad (7)$$

where C_T^* is the solvus concentration measured in mol/m^3 , V_m the volume of 1 mol of Al_3Sc , D the diffusion coefficient of Sc in the Al matrix, R the gas constant and T the temperature in K. Here, the estimates of the solvus line as given in Fig. 13 are used for calculating C_T^* , and the values of D are taken from [53]. Thus, by rearranging and solving Eq. (7) one gets an estimate of γ for each of the investigated transformation temperatures. The resulting values of the interface energy are plotted against transformation temperature in Fig. 14.

There is considerable spread in the obtained values of γ , which is attributed to the uncertainty in the determination of the rate constant k of Eq. (5). However, the estimates indicate a shift in γ values between 350 and 370 °C, and that the

² The right side of Eq. (6) is dimensionless, and the solvus concentration of Sc must thus be expressed as a dimensionless quantity as well, i.e. as an atomic fraction. However, both Fujikawa et al. [34], Torma et al. [40], Jo and Fujikawa [19] and Celotto and Bastow [33] use atomic percent when fitting their solvus measurements to the regular solution model. This introduces a deviation of $R \ln(100)$ in their reported values of ΔS compared to the present result (Table 5). If atomic fraction had been used instead, they would have obtained ΔS -values of 12, 15, 16 and 4 J/mol K, respectively.

Table 5
Estimates of ΔH and ΔS

Reference	$-\Delta H$ [kJ/mol]	ΔS [J/mol K]	Note
Fujikawa et al. (1979) [34]	59	50	
Hatch [39]	69.5	–	
Torma et al. (1985) [40]	63	53	
Jo and Fujikawa (1993) [19]	63	55	
Asta et al. (1998) [51]	72	–	Calculated
Hyland et al. (1998) [52]	64	–	Calculated
Celotto and Bastow (2000) [33]	52	42	
This work	65	19	

Unless otherwise noted, the estimates are made by fitting experimental solvus measurements to Eq. (6).

γ values decrease with increasing temperatures in the temperature intervals 190–350 and 370–510 °C. The interphase interface energy between Al and Al₃Sc has been estimated in several other publications. Reported values range from 10

[27] to approx. 200 mJ/m² [51]. In the theoretical calculations of [51,52] the interface energy is predicted to decrease somewhat with increasing temperature, but not to the extent that what is suggested by the present estimates.

The shift in γ values between 350 and 370 °C could be related to coherency loss at the particle/matrix interface at the higher temperature regime. Such loss of coherency is reported to occur when the Al₃Sc particles grow beyond a critical size [16,23,27,28,54], and an increase in the γ value due to the introduction of interfacial dislocations in continuously precipitated, spherical Al₃Sc particles has been reported [54]. It is also possible that the interfaces of discontinuously precipitated Al₃Sc particles have some properties that modify the γ value.

3.7. Deviation of solvus estimates at 350 °C and below

At temperatures of 350 °C and below, it is obvious that the solute content one calculates from the electrical conductivity at the end of the transformation is not the solvus concentration (Fig. 11). The apparent retained solute content increases with decreasing transformation temperature. Similar behaviour can also be seen in electrical conductivity/resistivity measurements published by numerous authors [16,19,23,25,27,32]. However, no convincing explanation for this behaviour has been found in the literature. In [25] it is suggested that the high supersaturation is due to the presence of metastable phases.

It is tempting to attribute this observation to the capillarity effect (Gibbs–Thomson effect). According to Porter and Easterling [50], the particle radius dependent solute content C_r varies with the mean particle radius r by the following relationship:

$$C_r = C_{Sc}^T \exp\left(\frac{2\gamma V_m}{RT r}\right) \quad (8)$$

where C_{Sc}^T is the solvus concentration at the temperature T , γ the interphase interface energy between Al and Al₃Sc and V_m the molar volume of the Al₃Sc phase.

No particle size measurements were made in this investigation. However, typical particle sizes have been reported elsewhere, thus giving a suggestion of what particle sizes one can expect. Rearranging Eq. (8) one gets the following

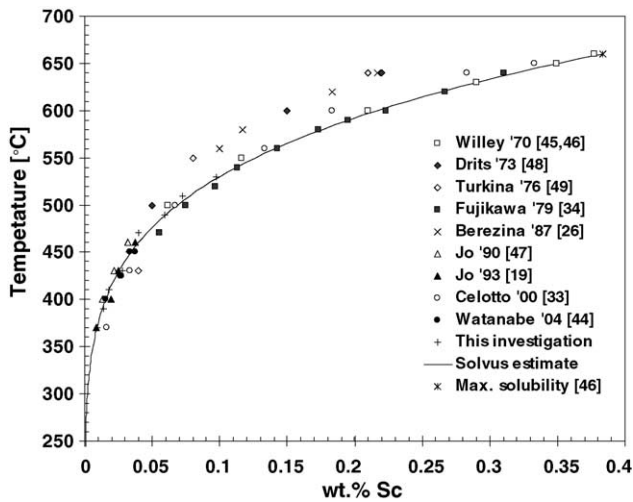


Fig. 13. Solvus line estimated from the present investigation along with previously reported solvus measurements.

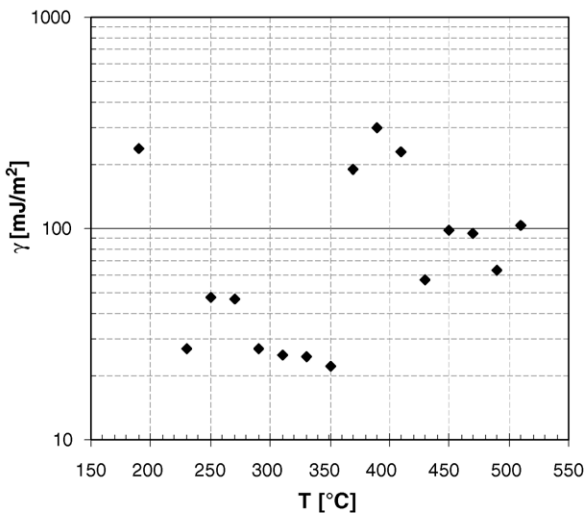


Fig. 14. Values of the interface energies achieved by using the experimental data to solve Eq. (7) for γ . The dotted lines are not regression lines but rather a suggestion of the general trend. Note the shift in γ for temperatures between 350 and 370 °C.

Table 6
Some measurements of the mean Al₃Sc particle diameter *d* after long time ageing

Reference	<i>d</i> [nm]	Note
Berezina et al. (1990) [27]	~10	Al–0.3 wt.% Sc, aged at 300 °C for 350 h (2 weeks)
Sano et al. (1990) [55]	18	Al–0.25 wt.% Sc, aged at 300 °C for 6 × 10 ⁵ s (1 week)
Miura et al. (1993) [56]	7.9	Al–0.23 wt.% Sc, aged at 350 °C for 10 ⁶ s (11.5 days)
Marquis and Seidman (2001) [57]	~6	Al–0.3 wt.% Sc, aged at 300 °C for 350 h (2 weeks)
Novotny and Ardell (2001) [58]	~30	Al–0.2 wt.% Sc, aged at 350 °C for 5 h–6 months

expression for the mean particle radius that would yield a specific supersaturation:

$$r = \frac{2\gamma V_m}{RT \ln(C_r/C_{Sc}^T)} \quad (9)$$

Assuming that $\gamma = 100 \text{ mJ/m}^2$, which is the overall average of the present estimates, and that the measured Sc-supersaturation is due to the capillarity effect only, one should find Al₃Sc particles with mean particle radii as given by the curve of Fig. 15. A second series of estimates based on the individual γ values of Fig. 14 is given by the black dots. One finds that at the lower temperatures, the mean particle radii would be approximately of the same size as the Al unit cell. Some typical particle sizes in Al–Sc alloys isothermally aged for long times, as reported by others [27,55–58] (see also Table 6), are included in Fig. 15. It seems clear that, even when accounting for the rough assumptions applied in this estimate, the measured supersaturation of Sc cannot be due only to the capillarity effect as described in Eq. (8). As far as one can see there are two other possibilities:

1. Provided that the electrical conductivity measurements give a reliable estimate of the solute content, the supersaturation of Sc must be due to other effects than the capillarity effect.

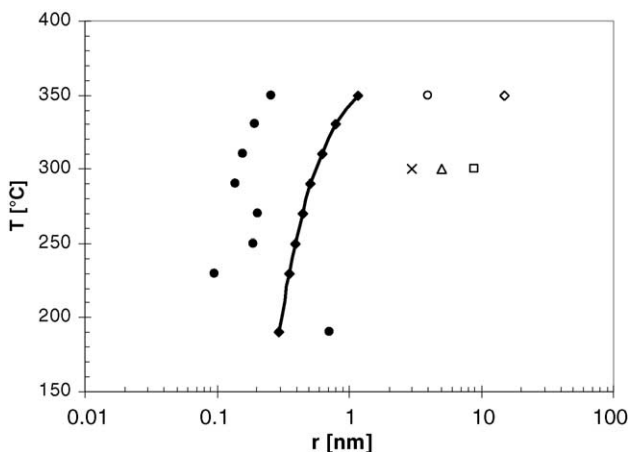


Fig. 15. Calculated radii that would explain the deviating solvus-measurements in terms of the capillarity effect. The solid line represents calculations with a fixed interface energy of 100 mJ/m², while the black dots are calculations based on the interface energy estimate for that specific temperature. The open symbols represent experimental observations: (Δ) Berezina et al. (1990) [27], (□) Sano et al. (1990) [55], (○) Miura et al. (1993) [56], (×) Marquis and Seidman (2001) [57], (◇) Novotny and Ardell (2001) [58].

2. Small Al₃Sc particles give a negative contribution to the electrical conductivity measurements, and thus lead to erroneous estimates of the solute content.

An interesting point can be made from Fig. 11. By extrapolating the curve of retained supersaturation to lower temperatures, it should cross the *C* value of 0.23 wt.% at a temperature somewhere between 50 and 150 °C. If the solute content is correctly estimated this means that at temperatures below the crossing point there can never be precipitation of Al₃Sc particles, and the electrical conductivity should be constant for infinite times. However, if the apparent retained solute content is an artefact from precipitate effects on the electrical conductivity there is a chance that ageing at temperatures below the crossing point gives a decrease, not an increase, in electrical conductivity when the Al₃Sc particles precipitate.

Thus, one should get some valuable input on this problem by doing long time annealing at low temperatures. The effect of isothermal ageing at 100 °C on electrical resistivity and hardness has already been reported [16,23,25] and no response was found. However, the maximum annealing time applied in these investigations (200 h) is probably shorter than what would be the incubation time for a precipitation reaction at this low temperature. A more thorough investigation in the low temperature range is needed if one wants to examine the hypothesis above.

It is interesting to note that in a recent investigation on the coarsening behaviour of an Al–0.3 wt.% Sc alloy [57] the estimated volume fraction of Al₃Sc particles after 72 h at 300 °C is less than half of the equilibrium volume fraction calculated from the phase diagram. In another investigation, where three-dimensional atom probe microscopy is used to count individual atoms after coarsening of an Al–Sc–Zr alloy at 300 °C, it is also found that the projected Sc and Zr content at infinite time is much higher than what is expected from the equilibrium diagram [59]. These observations sustain the suggestion that there may be an anomalous supersaturation of Sc after precipitation reactions in the low temperature range. However, no conclusions on this particular matter can be based on the available experimental results.

4. Conclusions

The precipitation process of an Al–0.23 wt.% Sc alloy, isothermally aged in the temperature range of 190–530 °C, has been followed by electrical conductivity measurements.

An estimate of the solute Sc content during the precipitation reaction was made from the conductivity measurements.

In the temperature range of 230–350 °C the precipitation reaction is well described by the JMAK equation when the transformed fraction is in the range of 5–95%. For temperatures in the range of 370–470 °C the precipitation reaction is divided in two distinct stages, a fast, early stage and a slow, late stage. For temperatures of 490 °C and above only one stage is observed.

Based on JMAK-plots of the isothermal transformations, a TTT-diagram was constructed for the temperature range of 230–510 °C. Two distinct transformation time minima are observed, one at approx. 310 °C and another one at approx. 410 °C.

Light microscope studies of specimens annealed at 450 °C indicate that discontinuous precipitation occurs in the first, rapid stage of transformation. This is confirmed by TEM observations. It is suggested that the first, rapid stage of transformation is dominated by discontinuous precipitation, and that the second, slow stage starts when the discontinuous precipitation comes to a halt.

Only continuous precipitation is observed in TEM after annealing at 350 °C.

Based on microstructural observations it is suggested that the transformation time minimum at approx. 310 °C is dominated by continuous precipitation, and that the transformation time minimum at approx. 410 °C is dominated by discontinuous precipitation.

A comparison with earlier work on the same alloy reveals that room temperature storage does not affect the precipitation rate as long as quenched-in vacancies are avoided.

From conductivity measurements of solutionized alloy and superpure aluminium, the resistivity of Sc in Al at room temperature was determined to be 29.7 nΩm/at.% Sc.

LSW theory was applied to the conductivity data from the coarsening stage of the precipitation reaction, and estimates of the solvus concentrations were made. For the temperature range of 370–530 °C the estimated values are within the spread of earlier reported values. For lower temperatures, however, the estimates are increasingly erroneous with lower transformation temperatures. Possible reasons for the error are discussed.

The coarsening data are also used for estimating the interface energy between Al and Al₃Sc. Although there is considerable spread of the estimates, from approx. 20 to 300 mJ/m², there seems to be some systematic variations with transformation temperature.

References

- [1] L.A. Willey, United States Patent no. 3619181 (November 9, 1971).
- [2] V.I. Elagin, V.V. Zakharov, T.D. Rostova, *Met. Sci. Heat Treatment* (1) (1992) 37–45.
- [3] V.V. Zakharov, *Met. Sci. Heat Treatment* 37 (1996) 283–285.
- [4] V.G. Davydov, V.I. Elagin, V.V. Zakharov, T.D. Rostova, *Met. Sci. Heat Treatment* 38 (1997) 347–352.
- [5] S. Kramer, W.T. Tack, M.T. Fernandes, in: *Proceedings of the Alumitech'97*, The Aluminum Association, USA, 1997, pp. 1231–1236.
- [6] H.G. Paris, T.H. Sanders Jr., Y.W. Riddle, in: T. Sato, S. Kumai, T. Kobayashi, Y. Murakami (Eds.), *Proceedings of the Sixth International Conference on Aluminum Alloys*, Japan Institute of Light Metals, 1998, pp. 499–504.
- [7] S.-I. Fujikawa, *J. Japan Inst. Light Met.* 49 (1999) 128–144.
- [8] A.F. Norman, P.B. Pragnell, R.S. McEwen, *Acta Mater.* 46 (1998) 5715–5732.
- [9] G.M. Khan, A.O. Nikiforov, V.V. Zakharov, I.I. Novikov, *Tsvetnye Metally* (11) (1993) 43–45.
- [10] M.G. Mousavi, C.E. Cross, Ø. Grong, *Sci. Technol. Weld. Joining* 4 (1999) 381–388.
- [11] J. Røyset, N. Ryum, in: T.H. Sanders Jr., E.A. Starke Jr. (Eds.), *Proceedings of the Fourth International Conference on Aluminum Alloys*, vol. I, Georgia Institute of Technology, School of Materials Science and Engineering, 1994, pp. 194–201.
- [12] J.S. Vetrano, S.M. Brummer, L.M. Pawlowski, I.M. Robertson, *Mater. Sci. Eng. A* 238 (1997) 101–107.
- [13] Y.W. Riddle, T.H. Sanders Jr., *Mater. Sci. Forum* 331–337 (2000) 799–804.
- [14] R.A. Emigh, E.L. Bradley, J.W. Morris Jr., in: E.W. Lee, N.J. Kim (Eds.), *Proceedings of the Conference on Light Weight Alloys for Aerospace Applications II*, TMS, 1991, pp. 27–43.
- [15] Z. Horita, M. Furukawa, M. Nemoto, A.J. Barnes, T.G. Langdon, *Acta Mater.* 48 (2000) 3633–3640.
- [16] M.Ye. Drits, L.B. Ber, Yu.G. Bykov, L.S. Toropova, G.K. Anastas'eva, *Phys. Met. Metall.* 57 (1984) 118–126.
- [17] N. Sano, Y. Hasegawa, K. Hono, H. Jo, K. Hirano, H.W. Pickering, T. Sakurai, *J. Phys. Colloq. C6* 48 (1987) 337–342.
- [18] R.W. Hyland Jr., *Met. Trans. A* 23 (1992) 1947–1955.
- [19] H.-H. Jo, S.-I. Fujikawa, *Mater. Sci. Eng. A* 171 (1993) 151–161.
- [20] N. Blake, M.A. Hopkins, *J. Mater. Sci.* 20 (1985) 2861–2867.
- [21] V.I. Elagin, V.V. Zakharov, T.D. Rostova, *Met. Sci. Heat Treatment* (6) (1993) 317–319.
- [22] J. Røyset, N. Ryum, in: T. Sato, S. Kumai, T. Kobayashi, Y. Murakami (Eds.), *Proceedings of the Sixth International Conference on Aluminum Alloys*, Japan Institute of Light Metals, 1998, pp. 793–798.
- [23] M.E. Drits, L.S. Toropova, U.G. Bikov, Anastaseva, in: F.J. Kedves, D.L. Beke (Eds.), *Proceedings of the DIMETA-82*, Trans. Tech. Publications, 1983, pp. 616–623.
- [24] V.I. Elagin, V.V. Zakharov, T.D. Rzzostova, *Met. Sci. Heat Treatment* (7) (1983) 546–549.
- [25] M.E. Drits, J. Dutkiewicz, L.S. Toropova, J. Salawa, *Cryst. Res. Technol.* 19 (1984) 1325–1330.
- [26] A.L. Berezina, V.A. Volkov, B.P. Domashnikov, K.V. Chuistov, *Metallfizika* 9 (5) (1987) 43–47.
- [27] A.L. Berezina, V.A. Volkov, B.P. Domashnikov, S.V. Ivanov, K.V. Chuistov, *Phys. Met.* 10 (1990) 296–304.
- [28] R. Wolter, P. Siebert, H.-G. Fabian, *Cryst. Res. Technol.* 28 (1993) 63–72.
- [29] S. Krause, G. Dlubek, H. Krause, A.L. Beresina, K.V. Chuistov, V.S. Mikhalev, *Phys. Stat. Sol. (a)* 141 (1994) 311–316.
- [30] M. Nakayama, A. Furuta, Y. Miura, *Mater. Trans. JIM* 38 (1997) 852–857.
- [31] V.V. Zakharov, *Met. Sci. Heat Treatment* 39 (1997) 61–66.
- [32] S.-I. Fujikawa, S. Sakauchi, in: T. Sato, S. Kumai, T. Kobayashi, Y. Murakami (Eds.), *Proceedings of the Sixth International Conference on Aluminum Alloys*, Japan Institute of Light Metals, 1998, pp. 805–810.
- [33] S. Celotto, T.J. Bastow, *Phil. Mag. A* 80 (2000) 1111–1125.
- [34] S.-I. Fujikawa, M. Sugaya, H. Takei, K.-I. Hirano, *J. Less-Common Met.* 63 (1979) 87–97.
- [35] *Aluminium-Taschenbuch*, 14. Auflage, Aluminium-Verlag, Düsseldorf, Germany, 1983.

- [36] M. Ocko, E. Babic, R. Krsmik, E. Girt, B. Leontic, *J. Phys. F: Metal Phys.* 6 (1976) 703–707.
- [37] A.S. Berger, *J. Less-Common Met.* 71 (1980) 119–126.
- [38] C. Papastaikoudis, D. Papadimitropoulos, *Phys. Rev. B* 24 (1981) 3108–3114.
- [39] J.E. Hatch, *Aluminum: Properties and Physical Metallurgy*, ASM, USA, 1984.
- [40] T. Torma, E. Kovács-Csetényi, I. Vitányi, M. Butova, J. Stepanov, in: *Proceedings of the Sixth International Symposium on High Purity Materials in Science and Technology*, Akademie der Wissenschaften der DDR, Dresden, GDR, 1985, pp. 388–389.
- [41] J.W. Christian, *The Theory of Transformation in Metals and Alloys*, 2nd ed., Pergamon Press, 1975.
- [42] A.J. Ardell, *Acta Met.* 15 (1967) 1772–1775.
- [43] A.J. Ardell, in: J.E. Morral, R.S. Schiffman, S.M. Merchant (Eds.), *Experimental Methods of Phase Diagram Determination*, TMS, 1994, pp. 57–66.
- [44] C. Watanabe, T. Kondo, R. Monzen, *Met. Mater. Trans. A* 35 (2004) 3003–3008.
- [45] L.A. Willey, Unpublished research, Alcoa, 1970, Data points are extracted from [46].
- [46] J.L. Murray, *J. Phase Equilib.* 19 (1998) 380–384.
- [47] H.-H. Jo, *J. Kor. Inst. Met.* 28 (1990) 499–504.
- [48] M.E. Drits, E.S. Kadaner, T.V. Dobotkina, N.I. Turkina, *Russ. Metall.* (4) (1973) 152–154.
- [49] N.I. Turkina, V.I. Kuzmina, *Russ. Metall.* (4) (1976) 179–183.
- [50] D.A. Porter, K.E. Easterling, *Phase Transformations in Metals and Alloys*, 2nd ed., Chapman & Hall, 1992.
- [51] M. Asta, S.M. Foiles, A.A. Quong, *Phys. Rev. B* 57 (1998) 11265–11275.
- [52] R.W. Hyland Jr., M. Asta, S.M. Foiles, C.L. Rohrer, *Acta Mater.* 46 (1998) 3667–3678.
- [53] S.-I. Fujikawa, *Defect Diffusion Forum* 143–147 (1997) 115–120.
- [54] S. Iwamura, Y. Miura, *Acta Mater.* 52 (2004) 591–600.
- [55] N. Sano, H. Jo, K. Hirano, T. Sakurai, in: C.Q. Chen, E. A. Starke Jr. (Eds.), *Proceedings of the Second International Conference on Aluminium Alloys*, International Academic Publishers, China, 1990, pp. 549–554.
- [56] Y. Miura, M. Nakayama, A. Furuta, in: Y. Hosoi, H. Yoshinaga, H. Oikawa, K. Maruyama (Eds.), *Proceedings of the Conference on Aspects of High Temperature Deformation and Fracture in Crystalline Materials*, The Japan Institute of Metals, 1993, pp. 255–262.
- [57] E.A. Marquis, D.N. Seidman, *Acta Mater.* 49 (2001) 1909–1919.
- [58] G.M. Novotny, A.J. Ardell, *Mater. Sci. Eng. A* 318 (2001) 144–154.
- [59] C.B. Fuller, J.L. Murray, D.N. Seidman, *Acta Mater.*, submitted for publication, 2005.